Flow, Turbulence and Combustion (2022) 109:515–543
https://doi.org/10.1007/s10494-022-00335-9

Multicomponent Effects on the Supercritical CO_2 Systems: Mixture Critical Point and Phase Separation

Hongyuan Zhang[1] · **Ping Yi**[1] · **Suo Yang**[1]

Received: 28 December 2021 / Accepted: 6 June 2022 / Published online: 27 June 2022

Abstract

Semi-closed supercritical CO_2 (sCO_2) gas turbine is a promising candidate for the next generation power cycles with high efficiency and almost 100% carbon capture. In this study, the multicomponent effects on the sCO_2 systems are investigated. A real-fluid modeling framework based on the vapor-liquid equilibrium (VLE) theory is implemented to predict the phase boundary and real mixture critical point, and to capture the phase separation in computational fluid dynamics (CFD) simulations. A novel VLE-based tabulation method is developed to make the CFD solver computationally more affordable. VLE-based thermodynamic analyses show that a small amount of combustion-relevant impurities (e.g., H_2O, CH_4, and O_2) can significantly elevate the mixture critical point of the sCO_2 systems. As a result, the so-called "supercritical" CO_2 systems might be in the subcritical two-phase zone where phase separation occurs. At the relevant conditions in this study (100–300 bar), phase separation only has a small influence on the $CO_2/H_2O/CH_4/O_2$ mixture density, but has a considerable influence on the heat capacity of the mixture. VLE-based CFD simulation of a laminar premixed sCO_2 shock tube shows that expansion waves can trigger significant condensation in the systems and the latent heat of the condensation can change the temperature and density fields in the systems. To understand the phase separation during mixing, VLE-based large-eddy simulations (LES) of turbulent jet-in-crossflows in the sCO_2 systems are conducted, and the results show that when two subcritical gas or supercritical gas-like streams mix, the mixture can partially condense to subcritical liquid phase. Higher pressure, lower temperature, and higher H_2O concentration can enhance the phase separation phenomenon in the systems.

Keywords Vapor–liquid equilibrium (VLE) · Multicomponent effects · Mixture critical point · Phase separation · Supercritical CO_2

✉ Suo Yang
suo-yang@umn.edu

[1] Department of Mechanical Engineering, University of Minnesota–Twin Cities, 111 Church Street SE, Minneapolis, MN 55455, USA

1 Introduction

Semi-closed supercritical carbon dioxide (sCO_2) oxy-combustion is a promising candidate for the next generation power cycles, since it is one of the potential solutions to effectively remove CO_2 and NO_x emissions from power generation. In a semi-closed sCO_2 cycle (see details in Appendix 1), the heat input typically comes from oxy-fuel combustion using either natural gas or syngas from a coal gasification process (McClung et al. 2015). This direct heating semi-closed sCO_2 power cycle can allow higher turbine inlet temperature than the indirect heating closed sCO_2 cycles to achieve higher efficiency. The NO_x emission is directly avoided by oxy-combustion (i.e., using pure oxygen rather than air as the oxidizer). The combustion products (primarily CO_2 and H_2O) can be recycled. In addition, since the high pressure sCO_2 holds high energy density, it can reduce the equipment size and improve the power density relative to air or oxygen (Dostal et al. 2004; Ahn et al. 2015). Although the advantages of the semi-closed sCO_2 gas turbine cycles are evident, the design of these cycles with oxy-combustion thermal input requires extensive knowledge of the real-fluid thermodynamics of multicomponent mixtures at a broad range of temperature and pressure conditions.

In the semi-closed sCO_2 cycles, impurities in CO_2 due to the combustion make it different from the traditional closed sCO_2 cycles, and the semi-closed sCO_2 cycles are no more single-component systems (Abdul-Sater et al. 2017; Barak et al. 2020). The impurities, especially components with high critical pressure such as H_2O, could significantly change the mixture critical point and phase boundary, and consequently, affect the thermodynamic proprieties of the working fluid. Hence, the thermodynamic characteristics of the mixture may deviate a lot from a single component. These effects may trigger phase separation, which may affect the system performance (e.g., thermal efficiency) and/or may cause safety issues. Thus, multicomponent effects on the sCO_2 systems (in terms of the effects of mixture critical point and phase separation) are important and need to be investigated.

1.1 Effects of Mixture Critical Point

Supercritical fluid, such as sCO_2, holds high energy density ρe near its mixture critical point due to the large variation of density ρ, which results in a large change in specific heat capacity c_p for a small temperature change. Therefore, it is better to keep the fluid temperature and pressure close to the mixture critical point to take this special advantage of high energy density to compact the turbomachinery. Accordingly, when designing and analyzing a semi-closed sCO_2 system, an accurate determination of the mixture critical point of a multicomponent mixture becomes very important.

1.2 Effects of Phase Separation

In the compressor of a semi-closed sCO_2 cycle, phase boundary change caused by multicomponent effects is a potential cause of phase separation. It may lead to compressor blade erosion, which has been widely investigated in traditional steam turbines (Ahmad et al. 2009) but not in sCO_2 gas turbines. In the sCO_2 oxy-combustor (i.e., the reactor in Fig. 17 of Appendix 1), phase separation caused by multicomponent effects may also occur due to the mixing between the working fluid (CO_2/H_2O) and injected O_2 and CH_4. For the pure gas phase, the mass mixing time scale is very small due to the large mass diffusivity, and the corresponding "effective" ignition delay is also short. For a two-phase state, due to the

presence of the liquid phase, the mass diffusivity is decreased, which increases the mass mixing time, but the thermal diffusivity is increased, which reduces the thermal conduction time. In these ways, multicomponent effects may affect the cold ignition in terms of "effective" ignition delay. In addition, phase separation may lead to combustion-induced Rapid Phase Transition (cRPT) (Basco et al. 2013), which causes anomalous high or oscillating pressures to damage the equipment and cause safety issues.

As mentioned above, multicomponent effects are important to understand the semi-closed sCO_2 gas turbine performance, such as thermal efficiency, compressor blade erosion, and "effective" ignition delays. However, very few researchers have investigated the influence of impurities (e.g., H_2O, CH_4, and O_2) on the sCO_2 systems (Vesely et al. 2019; Pint and Keiser 2018). To fill this scientific knowledge gap, the current fundamental study will focus on the multicomponent effects caused by impurities on the sCO_2 systems. But please note that the simulation and optimization of the real sCO_2 gas turbine systems (i.e., applied research) is out of the scope of this fundamental research and hence will not be covered in this paper.

Around the year of 2000, many important works have been done to simulation high-pressure supercritical fluids (Oefelein 2005; Bellan 2000; Yang 2000). These works majorly used "dense fluid" methods to describe the thermodynamic properties in the supercritical region. However, it cannot capture the phase change and multiphase effects (e.g., two-phase thermodynamic and transport properties) near the critical point. In order to investigate the multiphase thermodynamics of the sCO_2 systems, a vapor-liquid equilibrium (VLE) model (Michelsen 1982, 1987) is used in this study. The VLE model is based on the fundamental thermodynamics theory: Gibbs free energy is at a minimum at equilibrium. Hence, compared to low-pressure vaporization model, the VLE model is more suitable to capture phase boundary near the critical point. In this work, two VLE solvers [i.e., the isothermal-isobaric (TPn) flash solver (Michelsen 1982) and isobaric-isenthalpic (HPn) flash solver (Michelsen 1987)] are implemented, validated, and verified to predict the phase boundary and real mixture critical point, and simultaneously model the subcritical regime (with the consideration of phase change), the supercritical regime, as well as the transition between them. Thermodynamic and transport properties are evaluated based on the VLE solution, and thermodynamic relation are used to derive the formulas.

VLE model have been used for thermal analysis of various mixture systems. Xu et al. investigated high-pressure VLE at 293 K for $N_2/CH_4/CO_2$ systems (Xu et al. 1992). Perakis et al. modeled the VLE of the H_2O/ethanol/CO_2 system (Perakis et al. 2006). Pappa et al. modeled the VLE of the CO_2/H_2O system (Pappa et al. 2009). Silvia et al. analyzed the CO_2-based mixture, and improved accuracy by using an advanced mixing rule (Lasala et al. 2016). Legoix et al. investigated the mixtures of CH_4/CO_2 and $CH_4/CO_2/H_2O$ (Legoix et al. 2017). Although some CO_2-containing mixtures have been studied using VLE theory, before the present work, detailed VLE thermodynamics analysis of semi-closed sCO_2 systems has never been conducted in the literature, but such analysis is needed to better understand the sCO_2 system performance (e.g., thermal efficiency) and predict potential phase change which may affect ignition or cause safety issues.

Although the VLE theory has been proposed for a long while (Hanks et al. 1971) and 0D VLE calculation can be done by publicly available software such as the National Institute of Standards and Technology (NIST) REFPROP code (Lemmon et al. 2018), the development of VLE-based computational fluid dynamics (CFD) solvers to capture high-pressure phase change interacting with flow field just started during the past decade. (Matheis and Hickel 2018) integrated VLE models to a 3D compressible solver to reveal special breakup behaviors at supercritical conditions, which was also reported

in Roy and Segal's experimental results (Roy and Segal 2010) and Ana et al.'s simulation work (Star et al. 2006). Yao et al. used the tangent plane distance (TPD) method, a phase stability test method in VLE theory, to investigate the effect of mass diffusion model on phase stability (Yao et al. 2019). Ray et al. used the 2D compressible governing equation in the spherical coordinate system to describe droplet fluid dynamics, and integrated a VLE model to investigate the droplet evaporation at high pressures (Ray et al. 2019). Yi et al. developed a compressible four-equation model for multicomponent two-phase flow coupled with VLE solvers. Ma et al. integrated their non-conservative double-flux model (Ma et al. 2017) to a CFD solver, developed an adaptive scheme by coupling existing quasi-conservative and fully-conservative scheme, and analyzed the mixing behavior of fully conservative and quasi-conservative schemes (Ma et al. 2019). Tudisco and Menon developed the formula to handle VLE in multi-component mixtures (i.e., more than two components), and combined the non-conservative double-flux model (Ma et al. 2017) to a CFD solver to investigate the VLE effects on mixing flows (Tudisco and Menon 2020a). In addition, Tudisco and Menon (2020b) also developed a pρn VLE solver, and investigated the coupling between thermodynamic and transport properties and governing equations. Different from all the works above, this research integrated VLE solver with a CFD solver based on the PIMPLE algorithm (Holzmann 2016), which is a pressure-based scheme and suitable for "low-Mach" CFD simulation (but can also handle up to Mach 2 flows in its new transonic version). This work also developed a novel VLE-based tabulation method to make the VLE-based CFD solver computationally more affordable. This work develops a VLE-based CFD simulation framework by coupling a pressure-based CFD solver with the HPn flash solver to capture the phase separation in high-pressure multiphase flows. The thermodynamics analyses (of multicomponent mixtures) and CFD simulations (of a laminar premixed shock tube and turbulent jet-in-crossflows) are then conducted to reveal several mechanisms of phase separation in the sCO_2 systems.

The objectives of this research are:

- Understanding and quantifying the effects of combustion-relevant impurities (e.g., H_2O, CH_4, and O_2) on the mixture critical points and phase separation in the sCO_2 systems.
- Understanding and quantifying the effects of phase separation on different thermodynamic properties in the sCO_2 systems.
- Understanding the mechanisms of phase separation in premixed sCO_2 systems, particularly whether compression or expansion waves can trigger phase separation.
- Understanding the mechanisms of phase separation in non-premixed sCO_2 systems, particularly whether flow field and mixing processes can trigger phase separation.

The paper is structured as follows. Section 2 provides details of the numerical modeling, including the thermodynamics and transport models in Sect. 2.1 and the CFD framework in Sect. 2.2. Section 3 presents the results and discussion. Specifically, Sect. 3.1 presents the 0D analyses of the sCO_2 systems, including the influence of impurities on premixed sCO_2 systems in Sect. 3.1.1, the influence of mixture critical point and phase change on the thermodynamic properties in Sect. 3.1.2, and the isobaric and isenthalpic (HPn) mixing process in Sect. 3.1.3. Section 3.2 presents the 1D CFD simulation results of a laminar premixed sCO_2 shock tube. Section 3.3 presents the 3D large-eddy simulation (LES) results of turbulent jet-in-crossflows in the sCO_2 systems. Conclusions are summarized in Sect. 4.

2 Numerical Modeling

2.1 Models of Thermodynamics and Transport Properties

2.1.1 Models of Thermodynamics

This research investigated the systems of $CO_2/H_2O/CH_4/O_2$ mixtures. A conceptual schematic P–T diagram for the relevant multicomponent system in this study is shown in Fig. 1, which is relatively simple comparing to many other mixtures. The whole region is divided into liquid, gas, two-phase, and supercritical regions. In liquid, gas, and supercritical regions, only one phase is in the system. Peng–Robinson (PR) (Peng and Robinson 1976) cubic equation of state (EOS) and JANAF polynomials are used to evaluate thermodynamic properties. In the two-phase region, the vapor-liquid equilibrium (VLE) theory (Hanks et al. 1971) is need to determine phase fraction (i.e., the mole fraction of the gas phase) and compositions in the two phases, and then each phase uses the same model as above to evaluate thermodynamic properties. The mixture molar enthalpy and mixture compressibility factor are evaluated by blending (i.e., averaging weighted by phase fraction). Other thermodynamic properties are derived from relations between thermodynamic properties. Tudisco and Menon's work clearly discussed the relationship between properties and the associated calculation methods (Tudisco and Menon 2020), which are used in this work. Whether a system is in the two-phase region is also determined by VLE theory: If the gas mole fraction obtained by VLE theory is between 0 and 1, then the system falls into the two-phase region, and the equilibrium between vapor and liquid should be observed.

Two VLE solvers are implemented to solve the VLE problem numerically: the isothermal and isobaric (TPn) flash (Michelsen 1982) and isobaric and isenthalpic (HPn) flash (Michelsen 1987). TPn flash is the basic VLE solver, which solves the set of VLE equations at a given temperature (T), pressure (P), and mole fraction of each component (n) in the system. TPn flash is used for thermodynamic analysis and is also used for building other VLE solvers such as the HPn flash. HPn flash solves the VLE equation set at given enthalpy (H) rather than temperature. More details about these two VLE solvers can be found in Michelsen's works (Michelsen 1982, 1987) and the Supplementary Material. Tangent plane distance (TPD) method (Michelsen 1982) is used to ensure the correct convergence to the true VLE solution. The validation and verification of the VLE solvers are attached in Appendix 3.

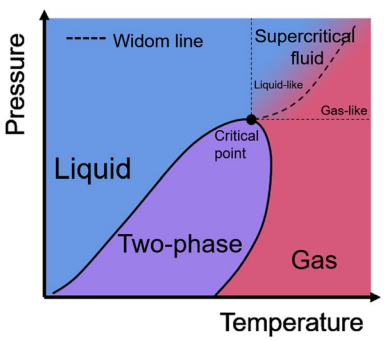

Fig. 1 A P–T Diagram for a multicomponent system

In semi-closed sCO_2 oxy-combustors, multiple fluids with different temperatures are mixed. There is almost no heat transfer to (or from) the surroundings, and except for pressure work, there is no other work done on (or by) the surroundings. Hence, the mixing of multiple fluids is isenthalpic (Serrano et al. 2018). Besides, the pressure does not change during the mixing processes. For these reasons, HPn flash is used to analyze the phase separation in the mixing processes in the sCO_2 systems.

2.1.2 Models of Transport Properties

The dense fluid formulas in the Chung's method (Chung et al. 1988) are used to evaluate the dynamic viscosity μ and thermal conductivity λ. Chung's method is accurate for polar (e.g., H_2O), non-polar (e.g., CO_2, CH_4, O_2) and associating pure fluids and their mixtures at high pressures (Chung et al. 1988). Meanwhile, its implementation is also straightforward. Chung's method has been widely used in a lot of studies of high pressure flows (Zhu and Reitz 2002; Trujillo et al. 2004; Yan and Aggarwal 2006; Matheis and Hickel 2018; Tudisco and Menon 2020b), and in software such as CoolProp (Bell et al. 2014) and REFPROP (Lemmon et al. 2018). For mas diffusivity D_m, the mixture-averaged mass diffusion model is used. Binary diffusion coefficient is evaluated by Fuller's model (Fuller et al. 1966) with Takahashi's correction (Takahashi 1975). Takahashi's correction (Takahashi 1975) is regarded as one of the most robust models at high pressures (Meng et al. 2005), and is widely used in high pressure flow simulations (Xu et al. 2018; Pohl et al. 2013; Nguyen et al. 2022; Ribert et al. 2017).

2.2 VLE-Based CFD Simulation Framework

In this study, a high-pressure multiphase flow simulation framework is developed by coupling a pressure-based CFD solver with a VLE solver (the HPn flash): i.e., a VLE-based CFD simulation framework. The CFD solver is based on multicomponent governing equations, including the continuity equation, mixture momentum equations, mixture specific internal enthalpy equation, and transport equations of distinct components in the mixture, as follows:

$$\frac{\partial \rho}{\partial t} + \frac{\partial \rho u_i}{\partial x_i} = 0 \tag{1}$$

$$\frac{\partial \rho u_i}{\partial t} + \frac{\partial \rho u_i u_j}{\partial x_j} = -\frac{\partial p}{\partial x_i} + \frac{\partial \tau_{ij}}{\partial x_j} \tag{2}$$

$$\frac{\partial \rho h}{\partial t} + \frac{\partial \rho u_i h}{\partial x_i} + \frac{\partial \rho K}{\partial t} + \frac{\partial \rho u_i K}{\partial x_i} - \frac{\partial p}{\partial t} = -\frac{\partial q_i}{\partial x_i} + \frac{\partial \tau_{ij} u_j}{\partial x_i} \tag{3}$$

$$\frac{\partial \rho Y_m}{\partial t} + \frac{\partial \rho Y_m u_j}{\partial x_i} = \frac{\partial}{\partial x_j}\left(\rho \sum_m D_m \frac{\partial Y_m}{\partial x_j} \right) \tag{4}$$

where u_i is the velocity, ρ and h are the mixture density and internal enthalpy, respectively, Y_m is the mass fraction of component m, p is the pressure, τ_{ij} is the viscous stress tensor, K is the kinetic energy, q_i is the heat flux, and D_m is the mass diffusivity of component m. In this study, $q_i = -\alpha \nabla h$ where α is the thermal diffusivity. In the relevant systems of this

study (mixture: $CH_4/CO_2/H_2O$, $O_2/CO_2/H_2O$; p: 10^7 Pa; T: 300–700 K), the Lewis numbers ($Le_m = \alpha/D_m$) are obtained using the models mentioned in Sect. 2.1, and their values are in the range of $O(10^3)$ to $O(10^5)$. Hence, the contribution of mass diffusion to energy flux is weak, and it is neglected in this study.

The OpenFOAM solver uses the PIMPLE algorithm (Holzmann 2016), which is a combination of the SIMPLE (semi-implicit method for pressure-linked equations) (Patankar and Spalding 1983) and PISO (pressure-implicit split-operator) algorithms (Issa 1986) based on the primitive variables (e.g., pressure p). The implementation of the PIMPLE algorithm in OpenFOAM has been validated by a lot of researchers around the world for different thermofluid applications (Robertson et al. 2015; Higuera et al. 2014; Gaikwad and Sreedhara 2019; Gamet et al. 2020; De Giorgi et al. 2017; Ashton and Skaperdas 2019). Additional validation and verification of the CFD solver are provided in Appendix 4, including two shock tube cases and a jet-in-cross flow case. In the original solver, the SIMPLE algorithm is used to predict ρ, u_i, h, and Y_m from Eqs. (1–4), in every time step (i.e., the outer loop in Fig. 2). Then, thermodynamic properties, including T (mixture temperature) and ϕ, are evaluated from the p in the last step and the updated h and Y_m using thermodynamic model. The ideal gas model and Peng-Robinson Equation of State, PR-EOS, are provided in the standard OpenFOAM version. ϕ is used to update p and calculate ρ. Then, transport properties are updated accordingly. Here, ϕ is defined as

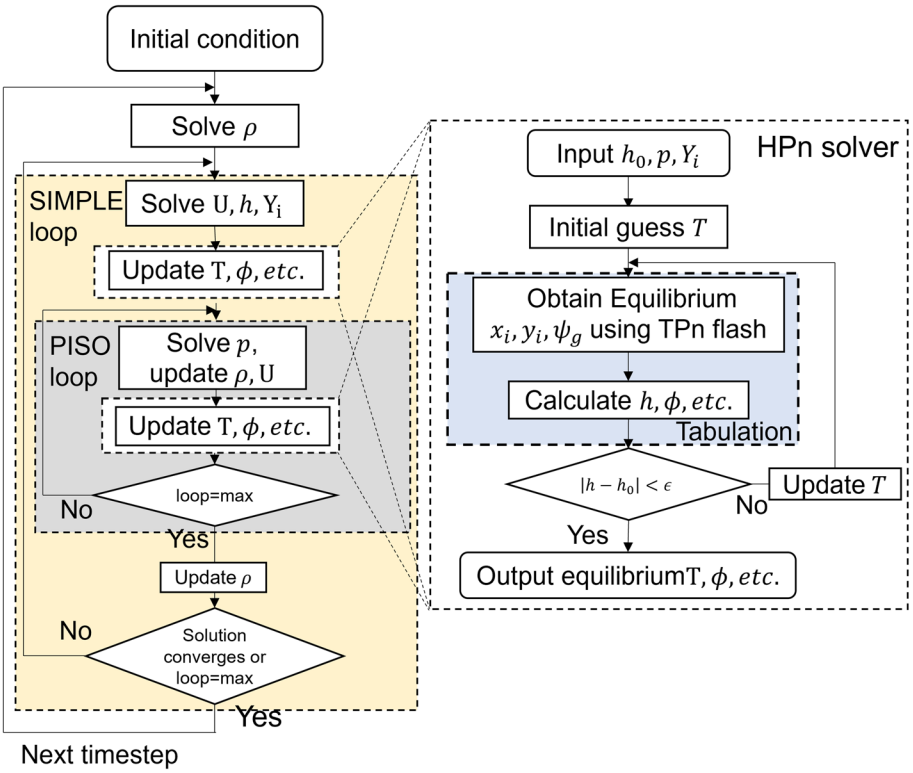

Fig. 2 Flow chart of the VLE-based CFD solver

$$\phi = \frac{\rho}{p}, \tag{5}$$

in which the specific form of ϕ depends on the choice of thermodynamics model. Then p is updated iteratively by solving its Poisson equation. Velocity u_i and thermodynamic properties (ρ, T, ϕ, etc.) are also updated after solving the pressure equation at each iteration step. This inner iteration is from the PISO algorithm, and hence it is called PISO loop, as shown in Fig. 2.

When PISO loop finshed, ρ is updated using Eq. (5). With the updated properties, Eqs. (2–4) are solved iteratively to update u_i, h, and Y_m, respectively, using the semi-implicit method (i.e., the predictor step) until it converges. This iteration is from the SIMPLE algorithm, and hence is called SIMPLE loop, as shown in Fig. 2. When SIMPLE loop finished, the next time step starts.

The new contributions from this study to the OpenFOAM solver and PIMPLE algorithm are summarized here. This study replaces the original thermodynamic model with the VLE+ PR-EOS model implemented in this study, as shown in Fig. 2. Due to the high computational cost of VLE calculation, a novel VLE-based tabulation method is developed to accelerate simulations and make the CFD solver computationally more affordable, as shown in the right box of Fig. 2. For each simulation, a table is generated to record the solution of TPn flash, density, enthalpy, c_p, and transport properties at different temperatures (280–1200 K), pressures (280–700 bar), and CO_2 mole fractions (0.0001–0.9999). Each solution includes, every species' mole fraction in liquid and gas phases, and transport properties. In simulations, a linear approximation method based on eight neighboring records is used for data retrieval. More details about this VLE-based tabulation method is provided in Appendix 2. For a large number of components, this tabulation method will demand infeasible memory, and we are developing a new on-the-fly tabulation of VLE solutions using the in situ adaptive tabulation (ISAT) approach (Zhang and Yang 2021), similar to the idea of correlated dynamic evaluation of real fluid properties for supercritical mixing (Yang et al. 2017) and combustion (Milan et al. 2019).

3 Results and Discussion

To investigate the effects of phase separation in sCO_2 systems, 0D thermodynamics analyses are first performed to discover the conditions under which phase separation could occur (in Sect. 3.1). In Sect. 3.2, 1D shock tube simulations are conducted to understand the effect of the phase change model compared with two models without phase change, and understand the interaction between phase separation and compression/expansion waves. In Sect. 3.3, we performed 3D jet-in-crossflow LES to discuss the influence of mixing on phase separation.

3.1 0D Thermodynamics Analyses of the sCO_2 Systems

In a real flow, many factors (e.g., boundary condition, turbulence, temperature perturbation) affect the fluid flow, making it difficult to analyze thermodynamic properties. Hence, in this section, 0D thermodynamics analyses are performed to give insights into the thermodynamic properties without the influence of other factors. First, the mixture critical points are calculated to show the influence of impurities in Sect. 3.1.1. Then, the influence

of the critical point on thermodynamic properties is discussed in Sect. 3.1.2. Since isenthalpic mixing is similar to what often happens in the real sCO_2 systems, in the end, the two-phase region in the isenthalpic mixing process is discussed (in Sect. 3.1.3).

3.1.1 Influence of Impurities on Premixed sCO_2 Systems: Elevated Critical Point and Retrograde Condensation

As discussed before, the injection of fuel (e.g., CH_4) and oxidizer (e.g., pure O_2 or air) and the combustion products (e.g., H_2O) can introduce many impurities to the sCO_2 systems. Accordingly, this section will investigate the mixture phase diagrams of sCO_2 systems with different combinations of impurities, including both two-component and three-component systems (also see Appendix 4 and Sect. 3.1.2 for four-component systems).

As an example of two-component sCO_2 systems, the pressure-temperature phase diagram of CO_2/H_2O mixtures is generated by the TPn flash solvers (Michelsen 1982) (see details in the Supplementary Material of this article) and shown in Fig. 3. The mixture critical pressures can be significantly higher than the critical pressure of each individual component (i.e., pure CO_2 and pure H_2O). As a result, at conditions close to the critical point of pure CO_2 (304.13 K, 73.78 bar), the CO_2/H_2O mixtures (with $\geq$ 10% H_2O) are in subcritical liquid phase. Therefore, a so-called "supercritical CO_2" system might be in a subcritical state due to the rise of mixture critical points caused by some impurities. In order to get a supercritical state for the CO_2/H_2O mixtures, the pressure and temperature need to be elevated about 100–200 K and 100–500 bar, respectively. In addition, retrograde condensation behavior could occur in such systems. Specifically, when the subcritical gas (at Point A) is compressed into the subcritical two-phase zone, phase separation could occur, and the gas partially condenses into liquid (at Point B), but further compression makes the mixture go outside of the two-phase zone such that the liquid component (at point B) evaporates again (i.e., the so-called "retrograde condensation") to Point C. Similar but the reverse process occurs during the expansion from Point C to Point A. As another example of two-component sCO_2 systems, Fig. 4a shows the thermodynamic states of CO_2/CH_4 mixtures. Similar to the CO_2/H_2O mixtures in Fig. 3, the mixture critical pressures of CO_2/CH_4 can also be higher than those of both pure CH_4 and pure CO_2.

As an example of three-component sCO_2 systems, Fig. 4 shows the influence of different levels of H_2O addition on the $CO_2/CH_4/H_2O$ mixture phase diagrams. As shown in Fig. 4b, even only 1% of H_2O addition can increase the mixture critical point significantly.

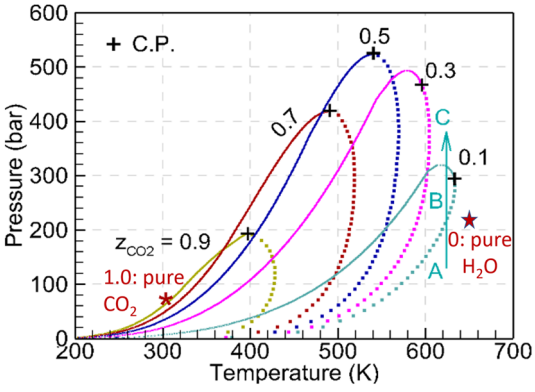

Fig. 3 Pressure–temperature phase boundaries and mixture critical points of CO_2/H_2O mixtures with different mole fraction values of CO_2 (i.e., z_{CO_2}). Note the retrograde condensation behavior from A to B to C

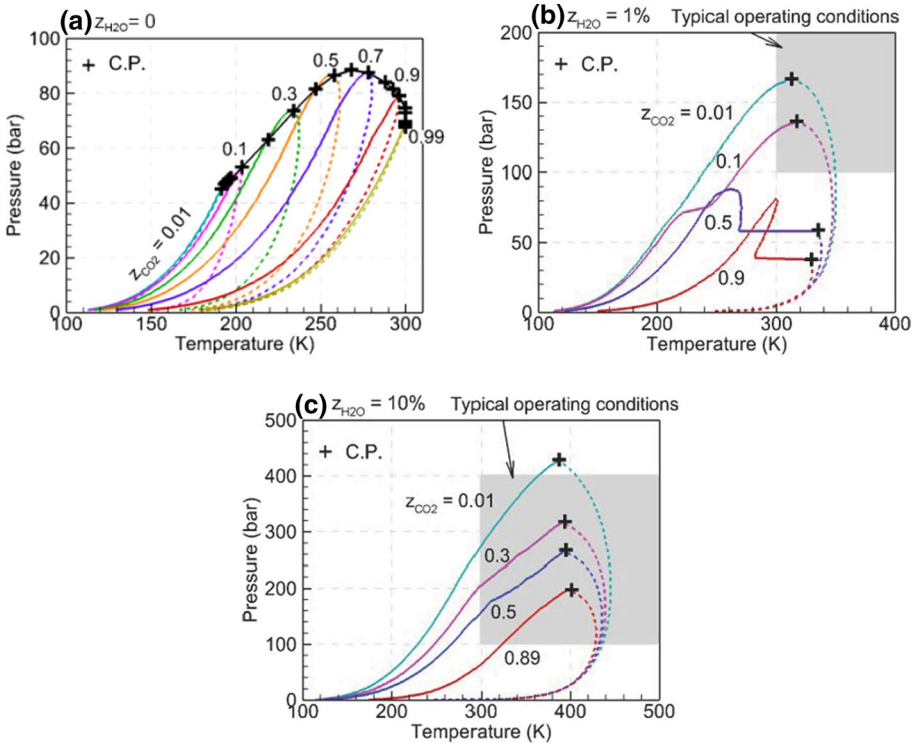

Fig. 4 Effects of H_2O addition on the pressure–temperature phase boundaries and critical points of CO_2 /CH_4/H_2O mixtures: **a** no H_2O addition; **b** 1% H_2O addition; **c** 10% H_2O addition

When the amount of CO_2 is sufficiently small (e.g., $z_{CO_2} \leq 0.1$), the mixture critical pressure can be larger than 100 bar. As shown in Fig. 4c, when z_{H_2O} rises to 10%, the mixture critical point increase even further. The mixture critical pressure can range from 200 to 400 bar. The typical working condition range of sCO_2 oxy-combustors (100–400 bar and $\geq$ 300 K) is indicated in Fig. 4. With H_2O addition, that working condition range overlaps with the subcritical two-phase zone, indicating that phase separation could occur. Another typical three-component sCO_2 systems are the CO_2/CH_4/O_2 systems, which are investigated in Appendix 4 and show similar retrograde condensation behavior as the CO_2/H_2O systems in Fig. 3.

3.1.2 Influence of Mixture Critical Point and Phase Change on the Thermodynamic Properties of the sCO_2 Systems

The mixture critical point and phase change affect all mixture thermodynamic properties, because all of them are functions of reduced pressure ($p_r = p/p_c$) and reduced temperature ($T_r = T/T_c$), especially when the thermodynamic state is close to the critical point and/or deviates from ideal gas (typically high p low T conditions).

Figure 5 shows the density of the mixture with and without phase separation. Comparing to the $z_{CO_2} = 0.9$ curve in Fig. 4b, it is seen that with the addition of O_2, the mixture critical pressure further rises from below 50 bar to approximately 350 bar. As a result, a significant part

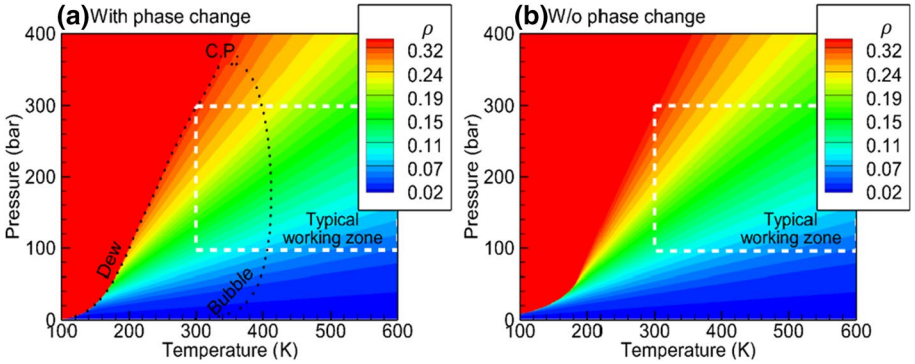

Fig. 5 Density (ρ) of $CO_2/H_2O/CH_4/O_2$ mixture with an overall mole fraction of 0.9/0.01/0.045/0.045 in the pressure–temperature phase diagram: **a** with phase change (i.e., with VLE); **b** without phase change (i.e., without VLE)

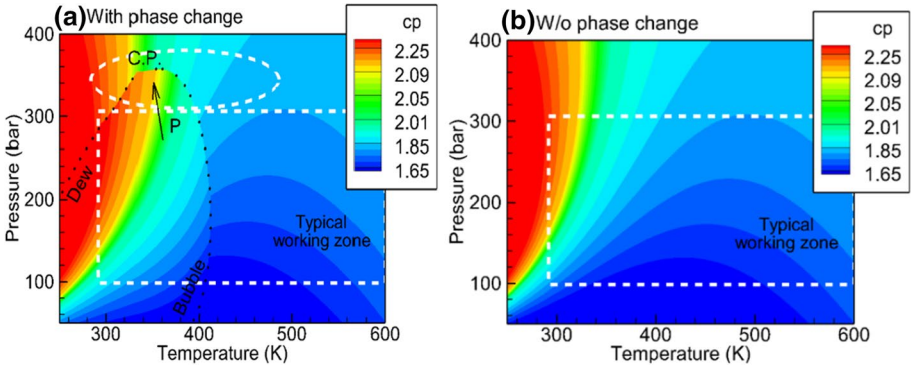

Fig. 6 Isobaric heat capacity (c_p) of $CO_2/H_2O/CH_4/O_2$ mixture with an overall mole fraction of 0.9/0.01/0.045/0.045 in the pressure-temperature phase diagram: **a** with phase change (i.e., with VLE); **b** without phase change (i.e., without VLE)

of the typical working conditions overlaps with the subcritical two-phase zone to trigger phase separation. By comparing Fig. 5a and b, it is seen that at the relevant conditions of this work (i.e., 100–300 bar), phase separation only has a small influence on the density of this specific mixture. This indicates that the assumption of "supercritical dense gas-like fluid" in Fig. 5b could result in a similar mixture density as the real subcritical two-phase mixture in Fig. 5a at the same thermodynamic condition.

In contrast, Fig. 6 shows that phase separation has a considerable influence on the isobaric heat capacity of the mixture. This could significantly affect the heating/evaporating time-scale of the mixture and consequently, affect the "effective" ignition delay in the cold ignition process.

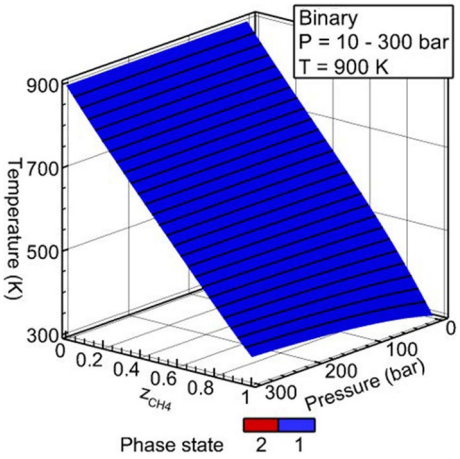

Fig. 7 Equilibrium mixing temperature T_{eq} for the mixing between 900 K CO_2 and 300 K CH_4: the pressure is in the range of 10–300 bar, and the overall mole fraction of CH_4 is in the range of 0.01–0.99. Red: two-phase zone; blue: single-phase zone

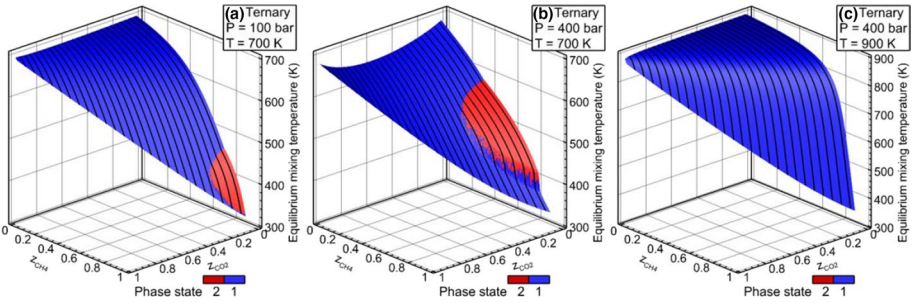

Fig. 8 Equilibrium mixing temperature T_{eq} for the mixing between CH_4 at 300 K and CO_2/H_2O mixture at the ambient pressure and temperature of **a** 100 bar and 700 K; **b** 400 bar and 700 K; and **c** 400 bar and 900 K. Red: two-phase zone; blue: single-phase zone

3.1.3 Isobaric and Isenthalpic (HPn) Mixing in the sCO_2 Systems: H_2O-induced Low-T Phase Separation

The previous analyses are based on the pressure-temperature phase diagrams generated by the isothermal and isobaric (TPn) flash solver (Michelsen 1982). However, many real mixing processes follow the isobaric and isenthalpic (HPn) path (Serrano et al. 2018). Thus the real phase states should be determined based on the isenthalpic mixing process generated by the HPn flash solver (Michelsen 1987). Details of both TPn and HPn flash solvers are provided in Michelsen's works (Michelsen 1982, 1987) and the Supplementary Material of this article.

Based on Fig. 7, for the mixing between 300 K CH_4 and 900 K CO_2 without H_2O, it is in a supercritical gas-like state during the whole mixing process, which agrees with the observation from the pressure-temperature phase diagram in Fig. 4a. Note that although not shown here, the same conclusion is observed when the ambient temperature of CO_2 is below 700 K.

As shown in Fig. 8, with the help of H_2O, the subcritical two-phase zone can start to play an important role. For the mixing between CH_4 (300 K) and CO_2/H_2O mixture, if the ambient temperature (i.e., the temperature of CO_2/H_2O mixture) is lower than 700 K (i.e., Fig. 8a,

b), the mixture can pass through the subcritical two-phase zone. The area of the two-phase zone increases as the pressure increases from 100 to 400 bar. When the ambient temperature reaches 900 K in Fig. 8c, the mixing process does not pass the subcritical two-phase zone, so there is no more phase separation. Hence, for sCO_2 systems with low temperatures (e.g., 700 K or lower), H_2O can cause phase separation. But for high-temperature sCO_2 systems (e.g., 900 K or higher), phase separation cannot happen.

3.2 1D Simulation of a Laminar Premixed sCO_2 Shock Tube: Condensation Driven by an Expansion Wave

Since semi-closed sCO_2 systems contain both compression and expansion processes (e.g., in the compressor stage and turbine stage, respectively), it is important to study the compression and expansion effects on real fluid and VLE. Shock tube is the simplest configuration to contain both compression and expansion processes, and hence is ideal to study those effects. In addition, sCO_2 shock tube is a common experimental facility to study semi-closed sCO_2 systems, whose designs require insights from computational studies. A shock tube case of a CO_2/H_2O mixture is tested at high-pressure conditions, which is used to compare different thermodynamics models. The initial condition is set close to the phase boundary to show the interaction between shock wave and phase change. As shown in Appendix 4, the CFD solver has been validated and verified by other shock tube cases. The initial condition of the current test case is shown in Table 1.

To show the importance of real-fluid EOS and VLE models in CFD simulations, three models are used and compared:

- ideal gas model;
- real-fluid model (PR-EOS) without phase change (i.e., without VLE);
- real-fluid model (PR-EOS) with phase change (i.e., with VLE).

From the pressure plot in Fig. 9a, it is apparent that the expansion wave in the PR-EOS model with VLE propagates slower, which is due to lower sound speed [with VLE: 312–323 m/s; without VLE: 363–378 m/s. The VLE sound speed is calculated based on the formula in Tudisco and Menon (2020)]. The phase equilibrium includes thermal equilibrium, mechanical equilibrium, and chemical equilibrium. In an isentropic process (i.e., $dS = 0$), when volume decreases (i.e., for a given $dV < 0$), these equilibria mitigate the pressure rise to minimize the total energy E and hence minimize the total energy rise ($dE = -pdV + TdS$). Consequently, with the same $\Delta\rho$, phase equilibrium makes p and hence the pressure rise Δp smaller than those without VLE. According to the formula of sounds speed $c = \sqrt{\left(\frac{\partial p}{\partial \rho}\right)_s}$, VLE causes the drop of sound speed. In Fig. 9b, because phase change is taken into account, latent heat is released when vapor partially condenses during the expansion wave propagation, which reduces the temperature reduction and makes PR-EOS with VLE have the highest

Table 1 Initial condition of a shock tube with CO_2/H_2O mixture

	P (bar)	T (K)	x_{CO_2}	x_{H_2O}
Left side	230	500	0.7	0.3
Right side	100	550	0.7	0.3

Domain length: 0.1 m; membrane location: 0.05

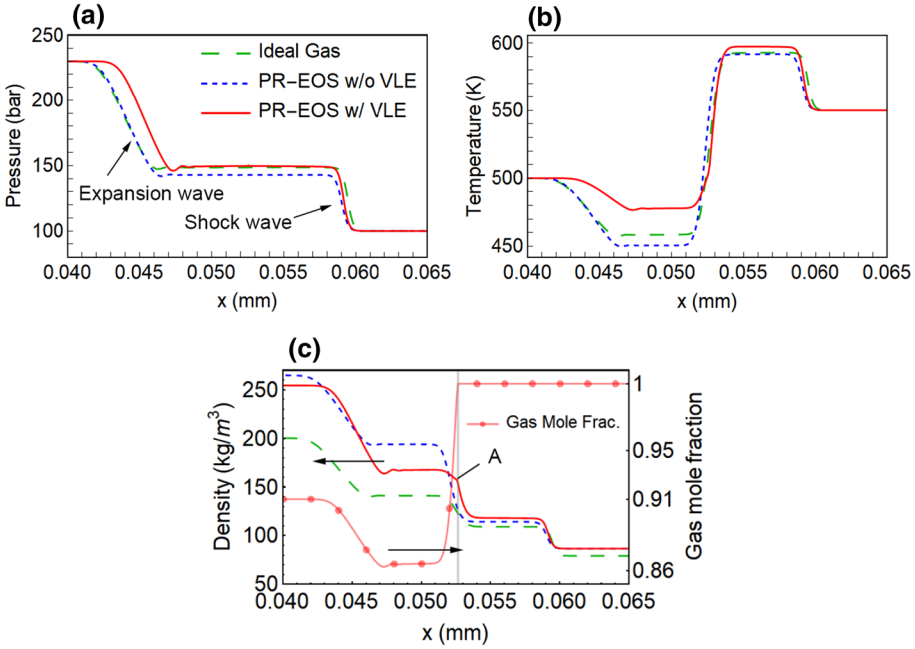

Fig. 9 Simulation results of a shock tube with CO_2/H_2O mixture, at $t = 2 \times 10^{-8} s$: **a** pressure; **b** temperature; **c** density and gas mole fraction

temperature. In Fig. 9c, the three models show evident differences in density prediction. Specifically, compared to the real-fluid models (PR-EOS), the ideal gas model underestimates the gas density. The effect of the phase change (i.e., VLE) increases the temperature in the expansion wave and hence reduces the density there. The gas mole fraction, predicted by the real-fluid model with phase change (i.e., with VLE) at different positions, indicates that the mixture is partially condensed after the expansion wave. Also, a sharp bend (point A) in the density line only exists in the prediction from the PR-EOS model with VLE, which corresponds to the location where the mixture starts to condense.

In summary, the real fluid model integrated with VLE can capture more physics caused by phase change. The results show that expansion waves can trigger significant condensation in premixed sCO_2 systems, and the latent heat of the condensation can change the temperature and density fields in the systems. Moreover, the speed of the expansion wave is reduced.

3.3 3D LES of Turbulent Jet-in-crossflows in the sCO_2 Systems: Mixing-Driven Phase Separation

To understand the mixing-driven phase separation in the sCO_2 systems (e.g., the fuel and oxidizer injections in sCO_2 oxy-combustors), large-eddy simulations (LES) of turbulent jet-in-crossflows are conducted. As shown in Appendix 4, the CFD solver based on the PIMPLE algorithm has been validated by another turbulent jet-in-crossflow case. In each simulation, cold (300 K) O_2 or CH_4 is injected from the nozzle at the bottom into hot (500 K or 700 K) CO_2 which contains a small amount of H_2O (10% or 20%).

Auto-ignition simulations at a constant pressure of 300 bar are conducted using Cantera (Goodwin et al. 2009) with GRI-Mech 3.0 (Smith 1999) as the chemical mechanism. Figure 10 shows that at 700 K the ignition delay is about 20 s, but the time scales of the mixing and phase separation processes of the jet-in-crossflow in this study are less than 1 ms. Moreover, the injected O_2 and CH_4 are at 300 K, which makes it difficult to have any obvious chemical effect. For these reasons, chemical reactions do not need to be considered at the conditions of this study.

More details about settings, geometry, and mesh are shown in Table 2 and Fig. 11. The mesh in the simulation contains 17.5M cells in total. The integral length scale l_0 is estimated using a Reynolds-averaged Navier–Stokes (RANS) simulation. $l_0 \approx 24$ μm in the interested region (0.4 cm $< x <$ 1.5 cm). The mesh in the interested region is refined to make sure $\Delta < l_0/5$, where Δ is the grid size and $\Delta \approx 3$ μm. When the above condition is satisfied, about 80% turbulent kinetic energy can be resolved by the mesh (the well-accepted criterion for LES resolution) (Gerasimov 2016), and hence the mesh resolution is high enough for LES (Pope 2004). Subgrid-scale (SGS) stress tensor is evaluated using the Smagorinsky model (Smagorinsky 1963). Since the VLE-based CFD of high-pressure multiphase flows is relatively new (more precisely, less than a decade), there is no investigation on the SGS mixing models of filtered VLE equations. Even the SGS mixing models for filtered real-fluid EOS are still not mature (Unnikrishnan

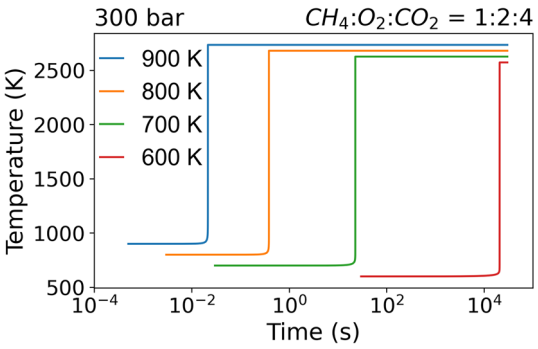

Fig. 10 Temperature vs. time plot: auto-ignition of $CH_4/O_2/CO_2$ system at a constant pressure of 300 bar. CH_4:O_2:CO_2 = 1:2:4, by mole

Table 2 Injection nozzle and inflow conditions of the turbulent jet-in-crossflows

p (bar)	T_{nozzle} (K)	T_{inflow} (K)	U_{nozzle} (m/s)	x_{H_2O}
300	300	500 or 700	300	0.2 or 0.1

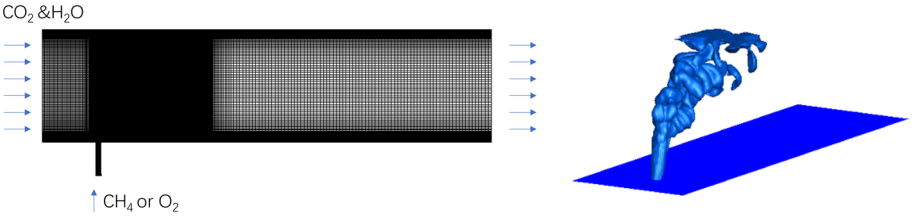

Fig. 11 Computational mesh and geometry of the turbulent jet-in-crossflows, and iso-surface of CO_2 mole fraction

et al. 2017, 2021). In this work, due to the limitations of the state-of-the-art, we do not consider the SGS terms of filtered VLE equations and filtered real-fluid EOS but will investigate them in the future.

Figure 12a–c shows the results of O_2 injection case. Near the injection nozzle, the cold O_2 is mixed with the hot CO_2/H_2O mixture: O_2 concentration keeps high as shown in Fig. 12a, and temperature keeps low as shown in Fig. 12b. In almost the same region, phase separation occurs as shown in Fig. 12c. The cold O_2 is in a supercritical gas-like state, and the hot CO_2/H_2O mixture is in the gas phase before they are mixed. However, the temperature of the injected O_2 is low enough to let the gaseous H_2O in the working medium (i.e., the CO_2/H_2O mixture) partially condense (i.e., the mixture enters the subcritical two-phase zone). With the mixing process proceeding, the low-temperature O_2 is diluted, and the mixture temperature goes up to the initial temperature of the CO_2/H_2O mixture (i.e., the ambient temperature). The small amount of H_2O in liquid phase quickly evaporate back to the gas phase. Hence, phase separation only appears near the injection nozzle, which agrees with the 0D thermodynamics analysis in Sect. 3.1.1. A similar phenomenon is also observed in the CH_4 injection case, as shown in Fig. 12(d). Compared with Fig. 12d, the jet in Fig. 12c bends less, and has stronger breakup, which is due to different density ratio $r = \rho_{jet}/\rho_{\infty}$ where ρ_{∞} is the density of the working medium (i.e., the CO_2/H_2O mixture) and ρ_{jet} is the density of the jet fluid from the injection nozzle. O_2 jet has higher density ratio ($r = 1.39$ from the data) than CH_4 jet ($r = 0.66$ from the data). The jet with higher density ratio trigger stronger breakup, which was also reported in Tretola et al. (2021).

It is worth noting that the phase separation condition is sensitive to the variation of ambient temperature. Here, two more simulations for both CH_4 and O_2 injections are conducted at 700 K ambient temperature. The gas fraction distributions of both cases are shown in Fig. 13. The phase separation phenomenon becomes much weaker in these two cases: the phase separation region and its gas mole fraction become much smaller. As a

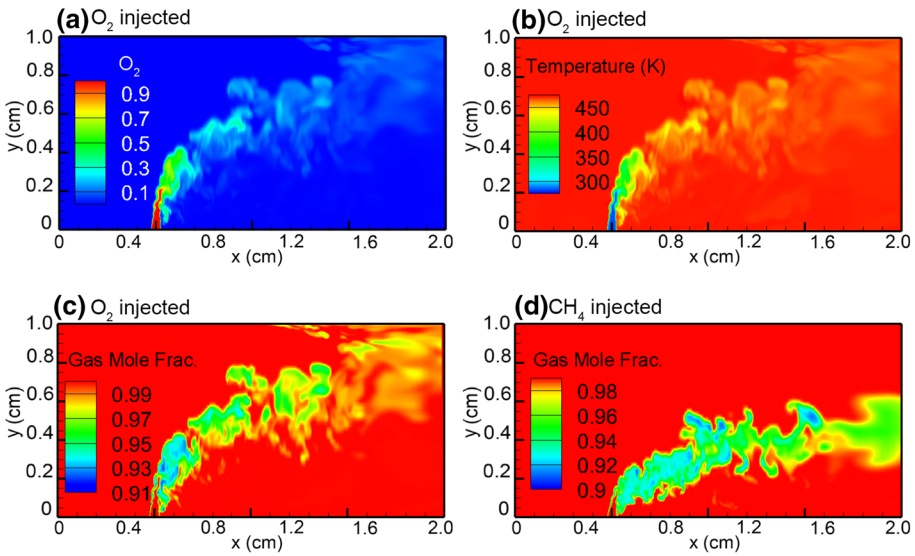

Fig. 12 LES of turbulent jet-in-crossflows (ambient temperature is 500 K, and the CO_2/H_2O mixture has 20% H_2O): **a** mole fraction of O_2 (O_2 is injected); **b** mixture temperature (O_2 is injected); **c** mole fraction of vapor (gas) phase (O_2 is injected); **d** mole fraction of vapor (gas) phase (CH_4 is injected)

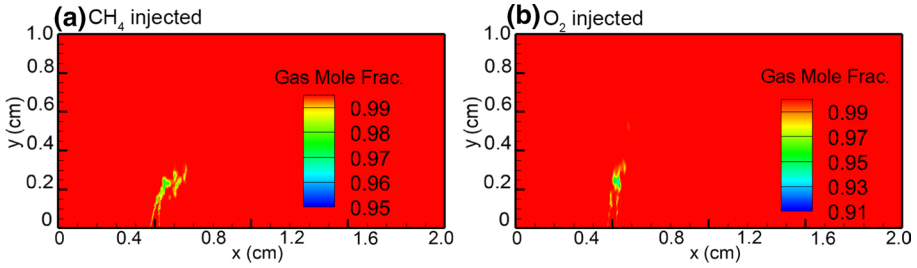

Fig. 13 LES of turbulent jet-in-crossflows (ambient temperature is 700K, the CO_2/H_2O mixture has 20% H_2O): **a** CH_4 is injected; **b** O_2 is injected

result, only a small portion of the mixture condenses and quickly evaporates back to the gas phase.

A better understanding of the mixing process and the influence of temperature can be obtained by the thermodynamics analysis of the LES data. In Fig. 14, subcritical two-phase and gas-phase regions are colored grey and white, respectively. The phase boundary shown in the plot is at 300 bar. Although the pressure varies in the flow field, the range (289–307 bar) is relatively small, which has almost no effect on phase boundaries, as shown in Fig. 15. Hence the phase boundary at 300 bar is a good representation of the boundaries of the system. The dots are the local thermodynamic states encountered in the LES, which form a curve (i.e., mixing trajectory) to connect the thermodynamic states of the injected fluid and the ambient CO_2/H_2O mixture. Since the dew point of CO_2 mixed with 20% H_2O is about 500 K, when the ambient temperature is 500 K, the mixing trajectory (green dots) is almost entirely inside the subcritical two-phase zone. When the ambient temperature increases to 700 K, one end of the trajectory of thermodynamic states moves upward, which can be seen clearly from the red dots in Fig. 14. As a result, only a small portion of the curve stays inside the subcritical two-phase zone, and phase separation can be observed only in a small region. The isenthalpic mixing lines are also marked in Fig. 14 to compare with the actual mixing trajectories. The difference between CH_4 injection and O_2 injection can be seen from the comparison between Fig. 14a and b. For the scenarios with CH_4 injection (Fig. 14a), at 500 K ambient temperature, the actual mixing trajectories almost overlaps with the isenthalpic lines,

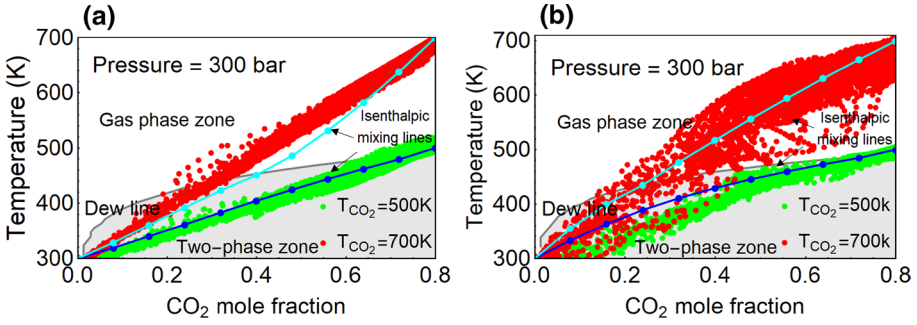

Fig. 14 Temperature-component diagrams of the LES data of two jet-in-crossflows: **a** injecting CH_4 into the CO_2/H_2O mixture with 20% H_2O; **b** injecting O_2 into the CO_2/H_2O mixture with 20% H_2O

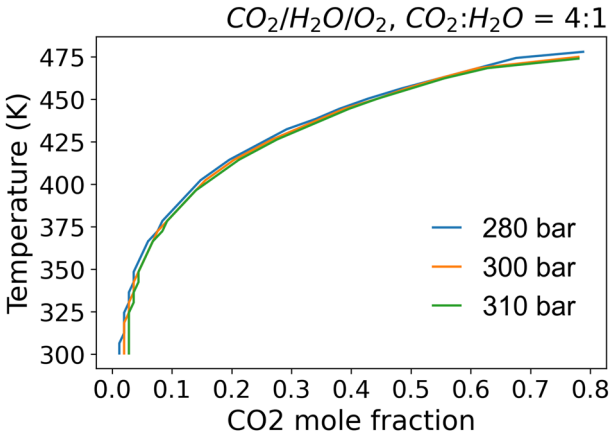

Fig. 15 Temperature-component diagrams of a $CO_2/H_2O/O_2$ system at 280 bar, 300 bar, 310 bar. CO_2:H_2O = 4:1, by mole

which is caused by weak thermal conduction; but at 700 K ambient temperature, larger temperature difference trigger stronger thermal conduction to raise the temperature, and hence the mixing temperature is mostly higher than the isenthalpic mixing temperature. Compared with Fig. 14a, the points in Fig. 14b are more dispersed, which is caused by higher density ratio (i.e., $r_{O_2} = 2.4$ is higher than $r_{CH_4} = 1.2$). Higher density ratio triggers stronger breakup, which enhances thermal conduction. Hence, more points deviate from the isenthalpic line. Although the properties of CH_4 and O_2 affect the dispersion of thermodynamic state points, they do not significantly affect the phase boundaries and the area of the phase separation region in the physical space.

Finally, the effect of H_2O addition is investigated. In this case, the ambient temperature is chosen as 500 K, and CO_2 contains 10% H_2O instead of 20% in the previous LES cases. Comparing Fig. 16a with the previous result in Fig. 12d, less H_2O leads to a smaller phase separation region. The mechanism behind this can be found in the phase diagram in Fig 16b. The mixing trajectories almost overlap with the isenthalpic lines. The mixture CO_2 with less H_2O has a lower dew line, and the high-temperature endpoint of the mixing trajectory moves out of the subcritical two-phase zone. The thermodynamic states of most fluid are near that endpoint. Hence, the subcritical two-phase zone in physical space is much smaller than the case with more H_2O.

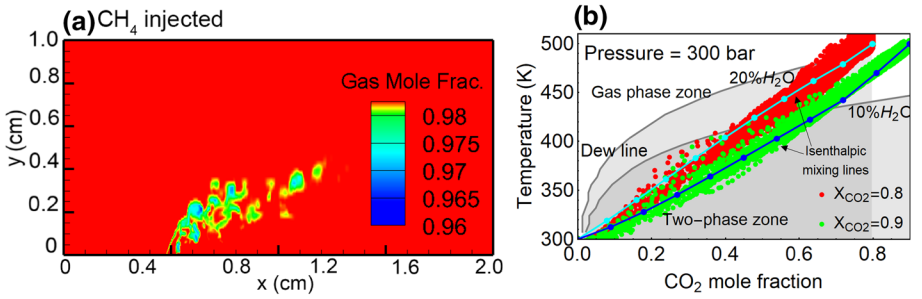

Fig. 16 **a** LES of turbulent jet-in-crossflow of injecting CH_4 into the CO_2/H_2O mixture with 10% H_2O (ambient temperature is 700 K): **a** gas mole fraction, and **b** temperature-component phase diagram

The conclusion is that when cold O_2 or CH_4 is injected into a hot mixture of CO_2 and H_2O, phase separation may occur. This phenomenon requires the CO_2/H_2O mixture to be close to the subcritical two-phase zone. Hence, ambient temperature and H_2O concentration have an evident influence on the phenomenon. Thermodynamics analysis can only tell whether there is phase separation. In contrast, when the thermodynamics analysis is combined with the CFD simulation, more insights can be obtained about the location and mole fraction of the liquid phase formed during the mixing.

4 Conclusion

In this study, the multicomponent effects on the supercritical CO_2 (sCO_2) systems are investigated. In order to investigate the multiphase thermodynamics of the sCO_2 systems, two vapor–liquid equilibrium (VLE) solvers (i.e., the isothermal–isobaric (TPn) flash solver and isobaric–isenthalpic (HPn) flash solver) are implemented, validated, and verified to predict the phase boundary and real mixture critical point, and simultaneously model the subcritical regime (with the consideration of phase change), the supercritical regime, as well as the transition between them. A VLE-based computational fluid dynamics (CFD) simulation framework is also developed by coupling a pressure-based CFD solver with the HPn flash solver to capture the phase separation in high-pressure multiphase flows. A novel VLE-based tabulation method is developed to make the CFD solver computationally more affordable. The thermodynamics analyses and CFD simulations are conducted to reveal several mechanisms of phase separation in the sCO_2 systems. The major findings include:

1. A small amount of combustion-relevant impurities (e.g., H_2O, CH_4, and O_2) can significantly elevate the mixture critical point of the sCO_2 systems, with a much higher critical pressure than that of each component of the mixture. As a result, the so-called "supercritical" CO_2 systems might be in the subcritical two-phase zone where phase separation (e.g., retrograde condensation) occurs. At the relevant conditions in this study (i.e., 100–300 bar), phase separation only has a small influence on the $CO_2/H_2O/CH_4/O_2$ mixture density, but has a considerable influence on the heat capacity of the same mixture.
2. For premixed sCO_2 systems (e.g., a premixed sCO_2 shock tube), evident effects of real fluid and phase separation are observed in expansion processes. Expansion waves can trigger significant condensation in premixed sCO_2 systems and the latent heat of the condensation can change the temperature and density fields in the systems. Moreover, the speed of the expansion wave is reduced by the phase separation.
3. Even without compression/expansion waves, mixing alone (e.g., in jet-in-crossflows) can raise the critical point such that the mixture can enter the subcritical two-phase zone to trigger phase separation. Specifically, when two subcritical gas or supercritical gas-like streams mix, the mixture can partially condense to subcritical liquid phase. Higher pressure, lower temperature, or higher H_2O concentration can enhance the mixing-driven phase separation phenomenon in the sCO_2 systems. In jet-in-crossflows, O_2 has higher density ratio than CH_4. Higher density ratio triggers stronger breakup, which enhances thermal conduction.

Appendix 1: Semi-closed sCO_2 Cycles

A cycle schematic of semi-closed sCO_2 gas turbine systems is shown in Fig. 17, which includes the following steps: The mixture of CO_2/H_2O with low temperature and low pressure (LTLP) is firstly compressed to a high temperature and high pressure (HTHP) state through the compressor. A cooler is used to remove a majority of the H_2O at high pressures. A remover is applied after the cooler to remove the excess CO_2 to conserve the mass in the cycle. The removed CO_2 can be diverted into a bypass stream to serve as a cooling flow around the head and walls of the oxy-combustor (i.e., the "reactor" in Fig. 17). Due to the loss of mass in the remover, the system pressure is reduced. A pump is used as compensation to increase the system pressure to a higher value. As the working fluid with moderate temperature and high pressure (MTHP) goes through a recuperator (i.e., a heat exchanger), the working fluid is heated to a high temperature by the exhaust gas mixture from the turbine. The working fluid enters the reactor (i.e., the oxy-combustor) and mixes with injected CH_4 and O_2. Then the auto-ignition occurs at around 900 K with high CO_2 concentrations. Herein, it must be noted that the so-called "supercritical" is defined based on the CO_2 critical point (P_c =73.8 bar, T_c =304.2 K) rather than the real mixture critical point.

Appendix 2: VLE-Based Tabulation Method

A tabulation method is used to accelerate VLE model computation. This method is used to replace the computationally expensive on-the-fly TPn flash. Within the given range of temperature, pressure, and mass fraction, TPn problems are solved on the evenly spaced grid points. Then the thermodynamic proprieties (including ρ, h, c_v, c_p) and transport proprieties (including D_m, μ, α) are evaluated using TPn solutions. The TPn solutions and all properties are recorded into the table. When retrieving the solution of given input (T^*, p^*, x^*), linear interpolation is used:

1. Find the closest temperature, pressure and mass fraction in the table, $T_1 \le T^* < T_2$, $p_1 \le p^* < p_2$, $x_1 \le x^* < x_2$
2. Calculate the weight for linear interpolation, $\alpha_1^v = \frac{v_2 - v^*}{v_2 - v_1}$, $\alpha_2^v = \frac{v^* - v_1}{v_2 - v_1}$, $v = T, p, x$

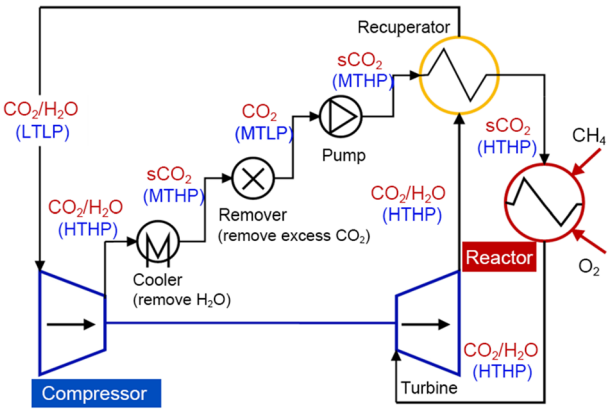

Fig. 17 Schematic of a sCO_2 gas turbine cycle with oxy-combustion thermal input

3. For any property A in the table, linear interpolation uses the formula $A^* = \sum_{i,j,k=1,2} \alpha_i^T \alpha_i^p \alpha_i^x A_{ijk}$

To mitigate the concern about potential VLE-inconsistency, an accuracy test is provided here. The same shock tube case as the one in Sect. 3.2 is used to test the tabulation method. The shock tube condition is shown in Table 1. The table used for the simulation covers the temperature range of 470–600 K, pressure range of 9–25 MPa, and x_{CO_2} range of 0.6–0.9. The table grid sizes are $\Delta T = 1.3$ K, $\Delta p = 0.4$ MPa, and $\Delta x_{CO_2} = 0.015$. The L^∞ absolute error (i.e., $max(\Delta A)$), maximum local relative error (i.e., $max(\frac{\Delta A}{A})$), and L^2 relative error (i.e., $\frac{\|\Delta A\|_{L^2}}{\|A\|_{L^2}}$) are obtained by comparing to the results without tabulation, and shown in Table 3. The results show that the maximum local errors are controlled within 10% and the L^2 errors are control within 5%.

Appendix 3: Validation and Verification of the VLE Solvers and CFD Solver

Validation of the TPn Flash Solver Based on Phase Boundaries

The TPn flash solver is validated by comparing the predictions with the experimental data of Somait and Kidnay (1978) in terms of the phase boundaries of CO_2/CH_4 and CO_2/H_2O mixtures. As shown in Fig. 18, the model prediction agrees with the experimental data very well for both mixtures.

Verification of the TPn Flash Solver Based on Mixture Critical Points

Next, the mixture critical points obtained from the VLE method (specifically, the TPn flash solver) are compared with those obtained from several other methods. In the VLE-based method, critical points can be obtained directly from the intersection of the dew curve and bubble curve.

Stradi et al. (2001) derived the mixture critical point based on Heidemann and Khalil's criticality formulation (Heidemann and Khalil 1980) as below, which has been widely used due to its clear theoretical foundation. For a mixture of C components,

$$Q\Delta \mathbf{n} = \mathbf{0} \tag{6}$$

Table 3 Relative error of VLE-based tabulation method

	Pressure	Density	Gas Mole Frac.
L^∞ absolute error	0.17 MPa	5.889 kg/m^3	0.02
maximum local relative error	1.4%	1.6%	2.1%
L^2 relative error	0.09%	0.09%	0.1%

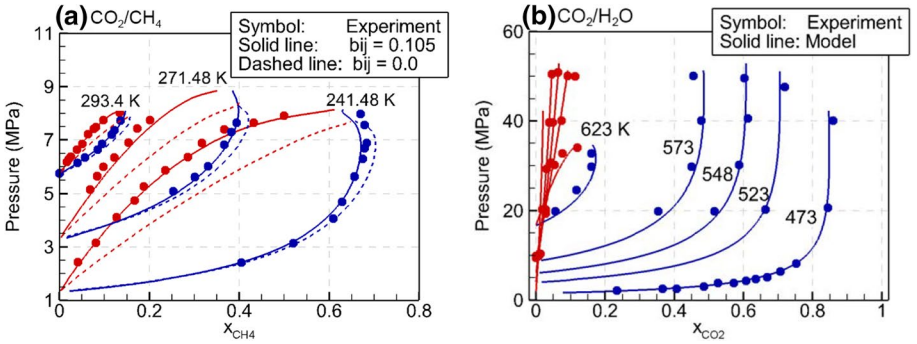

Fig. 18 Comparison of pressure-composition phase boundaries between experimental measurements and model predictions: **a** mixtures of CO_2 and CH_4; **b** mixtures of CO_2 and H_2O. Symbol: experimental data (Somait and Kidnay 1978); line: model prediction. In sub-figure **a**, solid line: binary interaction parameter $b_{ij} = 0.105$ is used in Eqs. (6–7) of the Supplementary Material; dashed line: $b_{ij} = 0$ is used in Eqs. (6–7) of the Supplementary Material. Red color: bubble points/curve, blue color: dew points/curve

$$Q_{ij} = \left(\frac{\partial^2 A}{\partial n_i \partial n_j} \right)_{T,V} \tag{7}$$

$$\sum_{i}^{C} \sum_{j}^{C} \sum_{k}^{C} A_{ijk} \Delta n_i \Delta n_j \Delta n_k = 0 \tag{8}$$

$$\Delta \mathbf{n}^T \Delta \mathbf{n} = 1 \tag{9}$$

$$A_{ijk} = \left(\frac{\partial^3 A}{\partial n_i \partial n_j \partial n_k} \right)_{T,V} \tag{10}$$

where $\Delta \mathbf{n}$ means the nonzero perturbation vector of the component mole numbers; A is the Helmholtz free energy. Since the Helmholtz free energy depends on the mixture composition, this way is implicitly dependent on the local mixture. The binary critical points predicted by the above methods are compared in Fig. 19, and the predictions of the current VLE-based method agree very well with Stradi et al.'s formulation (Stradi et al. 2001) for

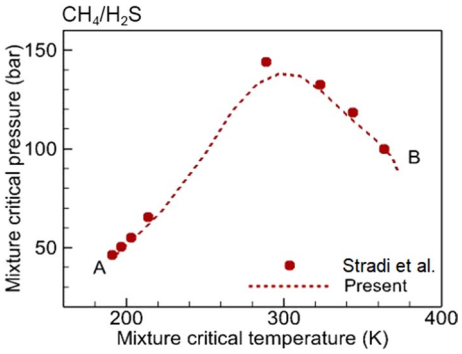

Fig. 19 Comparison of predicted mixture critical points of CH_4 /H_2S mixtures between (Stradi et al. 2001) and the present work (overall mole fraction of CH_4 is increased from 0.01 at A to 0.99 at B)

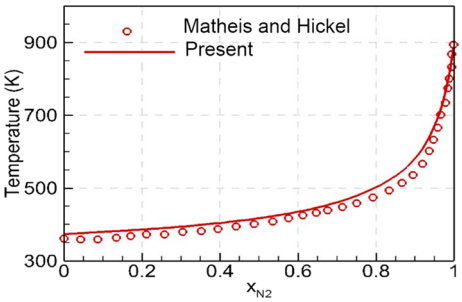

Fig. 20 Comparison of predicted equilibrium mixing temperatures T_{eq} for n-dodecane/nitrogen mixtures between (Matheis and Hickel 2018) and the current model

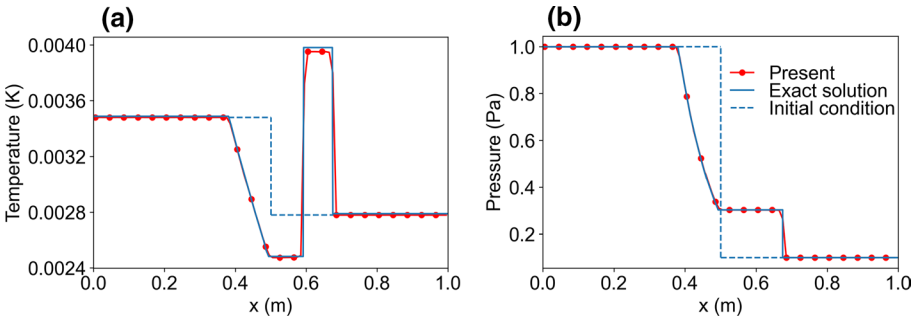

Fig. 21 Validation of the VLE-based CFD solver by Sod shock tube simulations. Initial conditions: $P_{\text{left}} = 1$ Pa, $P_{\text{right}} = 0.1$ Pa, $T_{\text{left}} = 0.00348$ K, $T_{\text{right}} = 0.00278$ K, the initial discontinuity is at $x = 0.5$ m; fluid: air; $t = 0.1$ s; 200 grid cells, CFL = 0.2

the mixture of CH_4 and H_2S. But note that Stradi et al.'s formulation can only predict critical points, and it cannot provide other detailed information (e.g., phase boundaries) about phase diagrams like what VLE solver can provide.

Verification of HPn Flash Solver Based on Equilibrium Mixing Temperature T_{eq}

All the validation and verification above are for the TPn flash solver. Here, the HPn flash solver is verified by the Fig. 1b in Matheis and Hickel (2018). As shown in Fig. 20, the present prediction of equilibrium mixing temperature T_{eq} agrees with Matheis and Hickel's result very well.

Validation and Verification of the CFD Solver

Two 1D shock tube simulations are conducted to validate and verify the CFD solver. First, Sod shock tube (Sod 1978) is used to test the CFD solver with the ideal gas model, and the results are shown in Fig. 21. The pressure and temperature evolution show a good agreement with the exact solution. Although the PIMPLE algorithm is pressure-based, the 1D Sod shock tube results clearly show that this compressible version of PIMPLE algorithm can well capture the shock wave and accurately predict compressible flows. Moreover, the results show that the scheme is not dissipative, as the sharp gradients (e.g., near the shock) are accurately captured with only 200 grid cells and there is no spurious oscillation near

the high gradients. Second, results from a shock tube simulation with phase change are compared with Chiapolino et al.'s simulation results (Chiapolino et al. 2017), as shown in Fig. 22. The shock tube is filled with a homogeneous water-air mixture, and the initial discontinuity is located at 0.5 m. Chiapolino et al.'s model used the Noble Abel Stiffened Gas (NASG) EOS and also assumed mechanical and thermodynamic equilibrium. Therefore, their results can also capture the phase change in the shock tube, which is valuable as a reference to verify the implementation of the VLE-based CFD simulation framework in this study both qualitatively and quantitatively. Good agreements were obtained in terms of the evolution of pressure and temperature at the contact discontinuity. Note that Chiapolino et al. used a fully compressible CFD solver (based on MUSCL Hancock method using van Leer's slope limiter and HLLC Riemann solver), while the CFD solver in this study uses a pressure-based PIMPLE method (which can be called a "low-Mach" solver but was extended to a transonic version). For this reason, the fact that both CFD solvers agree with each other can imply that the observed discrepancy between the CFD results with and without phase change (i.e., with and without VLE) in Fig. 9 should not come from numerical implementation but should come from the real physics of the shock tube problem.

LES of a jet-in-crossflow is also conducted to validate the CFD solver. The results are compared with Su and Mungal's experimental data (Su and Mungal 2004). The experiments were performed in an updraft wind tunnel with air as the crossflow fluid and nitrogen as the jet fluid. The crossflow and nitrogen are both at 300 K and 1 atm. Nitrogen is seeded with acetone vapor to 10% by volume for diagnostic purposes, which is also considered in the simulation. The tunnel crossflow velocity profile has a peak value of $v_\infty = 2.95$ m/s. Nitrogen is injected from a nozzle with inner diameter $d = 4.53$ mm, the jet average velocity is $u_0 = 16.9$ m/s. The mesh in the simulation contains 1.3M cells in total, and the average cell size is 2.3 mm. A finer mesh (500 μm) is used to capture the detailed flow structure near the injection nozzle. Based on the binary diffusivity of acetone and air ($D = 0.104$ cm^{2}s^{-1}) and the kinematic viscosity of air ($\nu = 0.155$ cm^{2}s^{-1}), Schmidt number, $Sc \equiv \nu/D$, of the system is 1.49. In Fig. 23, the center streamline and N_2 centerline of time-averaged field are compared between the simulation and experiments. The center streamline is the streamline that goes through the center of injector, and the N_2 centerline is the line of maximum N_2 concentration points at fixed-y planes. Length scales are

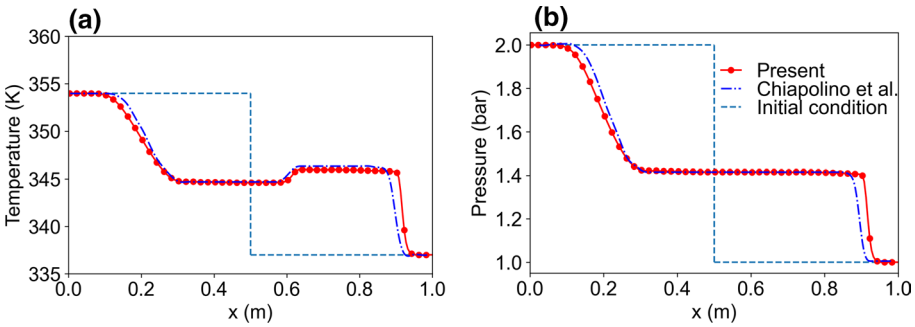

Fig. 22 Verification of the VLE-based CFD solver by Chiapolino et al.'s shock tube simulations (Chiapolino et al. 2017). Initial condition: $P_{\text{left}} = 2$ bar, $P_{\text{right}} = 1$ bar, $T_{\text{left}} = 354$ K, $T_{\text{right}} = 337$ K, $Y_{H_2O,\,\text{left}} = Y_{H_2O,\,\text{right}} = 0.3$, $Y_{\text{Air, left}} = Y_{\text{Air, right}} = 0.7$; $t = 1.0$ ms, 200 grid cells, CFL = 0.1, the initial discontinuity is at $x = 0.5$ m

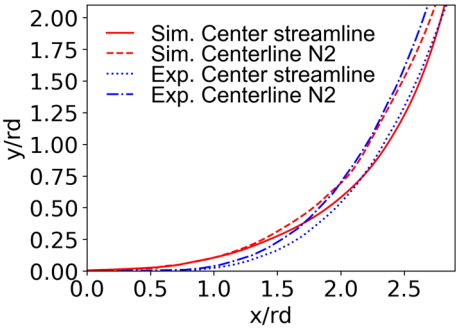

Fig. 23 Comparison of a jet-in-crossflow between the present model prediction and experimental data (Su and Mungal 2004). Blue: experimental data; red: simulation prediction

properly normalized by the factor rd, where d is the jet diameter (4.53 mm), r is ratio of jet velocity to crossflow velocity: $r \equiv u_0/v_\infty = 5.7$. The simulation results agree well with the experimental data at $x > 2rd$, but show a small deviation near the injection nozzle. This validation indicates that our CFD solver and LES models can accurately predict the mixing process at least for ideal gas.

Appendix 4: Influence of Different Diluents on Mixture Phase Diagrams

A key difference between the traditional gas turbine combustors and sCO_2 oxy-combustors is their different diluents: the former one has N_2 as its diluent, and the latter one has CO_2 as its diluent. When the removal of N_2 is incomplete, the sCO_2 oxy-combustor can also have a mixture of N_2 and CO_2 as its diluent.

Figure 24a shows the thermodynamic states of $CH_4/O_2/N_2$ mixtures. Close to pure air or pure fuel, the critical pressure is relatively low. The highest mixture critical pressure is reached at $z_{CH_4} = 0.6$. Also, note that even for the range of $z_{CH_4} < 0.6$, the trend of the mixture critical point is not monotonic (see the zoom-in figure), indicating that the real-fluid multiphase thermodynamics is highly nonlinear and any linear interpolation of mixture critical points is invalid. For all possible mixtures, the subcritical two-phase zone can only exist when the temperature is lower than 200 K.

Figure 24b shows the thermodynamic states of $CH_4/CO_2/O_2$ mixtures with or without N_2. When $z_{CO_2} \geq 0.6$, the influence of N_2 addition is very small; but when $z_{CO_2} \leq 0.5$, N_2 addition can significantly increase the mixture critical pressure. By comparing Fig. 24b to a, it is observed that CO_2 addition can significantly increase the mixture critical pressure. However, at typical operating conditions of sCO_2 oxy-combustion (100–400 bar and $\geq$ 300 K), the mixtures are still in supercritical gas-like or subcritical gas states, because the subcritical two-phase zone exists only when the temperature is lower than 300 K.

As shown by Fig. 24c, retrograde condensation behavior can also occur in the $CO_2/CH_4/O_2$ systems, similar as the CO_2/H_2O systems in Fig. 3.

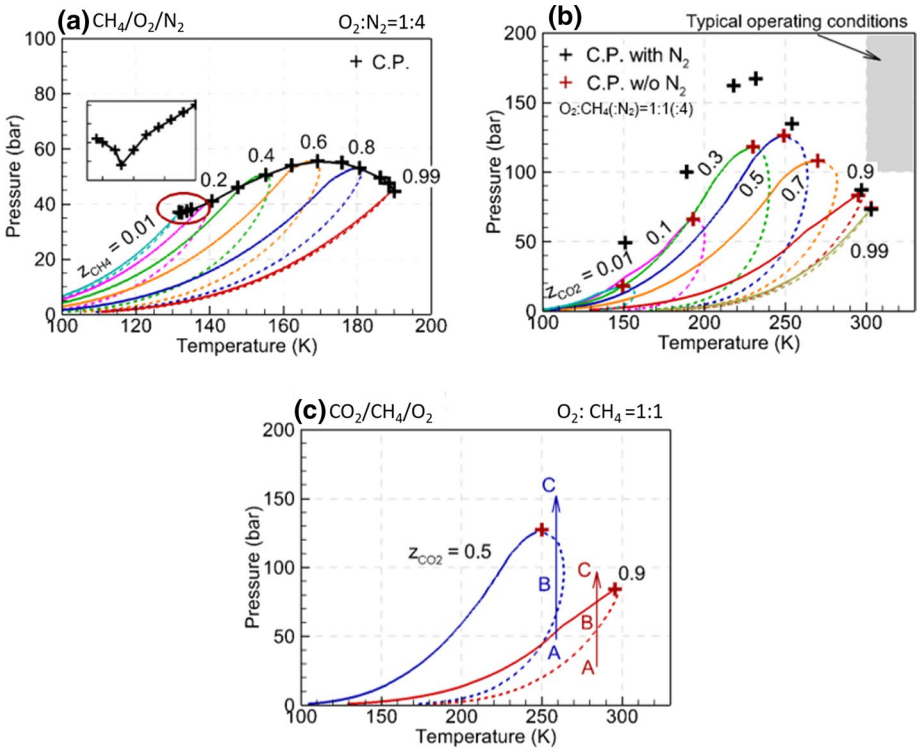

Fig. 24 Pressure–temperature phase boundaries and critical points of different mixtures: **a** $CH_4/O_2/N_2$, in which O_2:N_2=1:4 (which is close to the air composition); **b** $CO_2/CH_4/O_2(/N_2)$, in which O_2:CH_4(:N_2)=1:1(:4); **c** $CO_2/CH_4/O_2$, in which O_2:CH_4=1:1. Note the retrograde condensation behavior from A to B to C

Supplementary Information The online version contains supplementary material available at https://doi.org/10.1007/s10494-022-00335-9.

Acknowledgements S. Yang gratefully acknowledges the support from the faculty start-up funding from the University of Minnesota, the National Science Foundation (NSF) grant under Award No. CBET 2023932, and the Office of Naval Research (ONR) Grant under Award No. N00014-22-1-2287 under the supervision of project monitor Dr. Steven Martens. H. Zhang gratefully acknowledges the support from the 3M Science and Technology Doctoral Fellowship, UMII MnDRIVE Graduate Assistantship Award, and Frontera Computational Science Fellowship. The authors gratefully acknowledge the computing resources provided by the Minnesota Supercomputing Institute (MSI), Prof. Graham V. Candler, and Texas Advanced Computing Center (TACC).

Declarations

Conflict of interest The authors declare that they have no conflict of interest.

References

Abdul-Sater, H., Lenertz, J., Bonilha, C., Lu, X., Fetvedt, J.: Turbo Expo: Power for Land, Sea, and Air, vol. 50848, p. V04AT04A051. American Society of Mechanical Engineers, New York (2017)

Ahmad, M., Casey, M., Sürken, N.: Experimental assessment of droplet impact erosion resistance of steam turbine blade materials. Wear **267**(9–10), 1605–1618 (2009)

Ahn, Y., Bae, S.J., Kim, M., Cho, S.K., Baik, S., Lee, J.I., Cha, J.E.: Review of supercritical CO_2 power cycle technology and current status of research and development. Nucl. Eng. Technol. **47**(6), 647–661 (2015)

Ashton, N., Skaperdas, V.: Verification and validation of openfoam for high-lift aircraft flows. J. Aircr. **56**(4), 1641–1657 (2019)

Barak, S., Pryor, O., Ninnemann, E., Neupane, S., Vasu, S., Lu, X., Forrest, B.: Ignition delay times of oxy-syngas and oxy-methane in supercritical CO_2 mixtures for direct-fired cycles. J. Eng. Gas Turbines Power **142**(2), 021014 (2020)

Basco, A., Cammarota, F., Di Benedetto, A., Di Sarli, V., Salzano, E., Russo, G.: The effect of the hydrogen presence on combustion-induced rapid phase transition of $CO/O_2/N_2$ mixtures. Int. J. Hydrog. Energy **38**(36), 16,463-16,470 (2013)

Bell, I.H., Wronski, J., Quoilin, S., Lemort, V.: Pure and pseudo-pure fluid thermophysical property evaluation and the open-source thermophysical property library coolprop. Ind. Eng. Chem. Res. **53**(6), 2498–2508 (2014)

Bellan, J.: Supercritical (and subcritical) fluid behavior and modeling: drops, streams, shear and mixing layers, jets and sprays. Prog. Energy Combust. Sci. **26**(4–6), 329–366 (2000)

Chiapolino, A., Boivin, P., Saurel, R.: A simple and fast phase transition relaxation solver for compressible multicomponent two-phase flows. Comput. Fluids **150**, 31–45 (2017)

Chung, T.H., Ajlan, M., Lee, L.L., Starling, K.E.: Generalized multiparameter correlation for nonpolar and polar fluid transport properties. Ind. Eng. Chem. Res. **27**(4), 671–679 (1988)

De Giorgi, M.G., Ficarella, A., Fontanarosa, D.: Implementation and validation of an extended Schnerr–Sauer cavitation model for non-isothermal flows in openfoam. Energy Procedia **126**, 58–65 (2017)

Dostal, V., Driscoll, M.J., Hejzlar, P.: A supercritical carbon dioxide cycle for next generation nuclear reactors. Ph.D. thesis, Massachusetts Institute of Technology, Department of Nuclear Engineering (2004)

Fuller, E.N., Schettler, P.D., Giddings, J.C.: New method for prediction of binary gas-phase diffusion coefficients. Ind. Eng. Chem. **58**(5), 18–27 (1966)

Gaikwad, P., Sreedhara, S.: Openfoam based conditional moment closure (CMC) model for solving non-premixed turbulent combustion: Integration and validation. Comput. Fluids **190**, 362–373 (2019)

Gamet, L., Scala, M., Roenby, J., Scheufler, H., Pierson, J.L.: Validation of volume-of-fluid openfoam® isoadvector solvers using single bubble benchmarks. Comput. Fluids **213**, 104 (2020)

Gerasimov, A.: Quick guide to setting up les-type simulations. ANSYS Sweden AB, Goteborg (2016)

Goodwin, D.G., Moffat, H.K., Speth, R.L.: Cantera: An Object-Oriented Software Toolkit for Chemical Kinetics, Thermodynamics, and Transport Processes. Caltech, Pasadena (2009)

Hanks, R.W., Gupta, A.C., Christensen, J.J.: Calculation of isothermal vapor–liquid equilibrium data for binary mixtures from heats of mixing. Ind. Eng. Chem. Fundam. **10**(3), 504–509 (1971)

Heidemann, R.A., Khalil, A.M.: The calculation of critical points. AIChE J. **26**(5), 769–779 (1980)

Higuera, P., Lara, J.L., Losada, I.J.: Formulation and validation. Three-dimensional interaction of waves and porous coastal structures using openfoam®. Part I. Coastal Eng. **83**, 243–258 (2014)

Holzmann, T.: Mathematics, Numerics, Derivations and Openfoam®. Holzmann CFD, Loeben (2016)

Issa, R.I.: Solution of the implicitly discretised fluid flow equations by operator-splitting. J. Comput. Phys. **62**(1), 40–65 (1986)

Lasala, S., Chiesa, P., Privat, R., Jaubert, J.N.: Vle properties of CO_2-based binary systems containing N_2, O_2 and Ar: experimental measurements and modelling results with advanced cubic equations of state. Fluid Phase Equilib. **428**, 18–31 (2016)

Legoix, L.N., Ruffine, L., Donval, J.P., Haeckel, M.: Phase equilibria of the CH_4–CO_2 binary and the CH_4–CO_2–H_2O ternary mixtures in the presence of a CO2-rich liquid phase. Energies **10**(12), 2034 (2017)

Lemmon, E., Bell, I.H., Huber, M., McLinden, M.: Nist standard reference database 23: Reference fluid thermodynamic and transport properties-refprop, version 10.0, national institute of standards and technology. Standard Reference Data Program, Gaithersburg (2018)

Ma, P.C., Lv, Y., Ihme, M.: An entropy-stable hybrid scheme for simulations of transcritical real-fluid flows. J. Comput. Phys. **340**, 330–357 (2017)

Ma, P.C., Wu, H., Banuti, D.T., Ihme, M.: On the numerical behavior of diffuse-interface methods for transcritical real-fluids simulations. Int. J. Multiph. Flow **113**, 231–249 (2019)

Matheis, J., Hickel, S.: Multi-component vapor–liquid equilibrium model for les of high-pressure fuel injection and application to ecn spray a. Int. J. Multiph. Flow **99**, 294–311 (2018)

McClung, A., Brun, K., Delimont, J.: Turbo Expo: Power for Land, Sea, and Air, vol. 56802, p. V009T36A006. American Society of Mechanical Engineers, New York (2015)

Meng, H., Hsiao, G., Yang, V., Shuen, J.: Transport and dynamics of liquid oxygen droplets in supercritical hydrogen streams. J. Fluid Mech. **527**, 115–139 (2005)
Michelsen, M.L.: The isothermal flash problem. Part I. Stability. Fluid Phase Equilib. **9**(1), 1–19 (1982)
Michelsen, M.L.: Multiphase isenthalpic and isentropic flash algorithms. Fluid Phase Equilib. **33**(1–2), 13–27 (1987)
Milan, P.J., Li, Y., Wang, X., Yang, S., Sun, W., Yang, V.: 11th US National Combustion Meeting, 71TF, 396 (2019), 1–10
Nguyen, D.N., Jung, K.S., Shim, J.W., Yoo, C.S.: Real-fluid thermophysicalmodels: an openfoam-based library for reacting flow simulations at high pressure. Comput. Phys. Commun. **273**, 108,264 (2022)
Oefelein, J.C.: Thermophysical characteristics of shear-coaxial lox-H_2 flames at supercritical pressure. Proc. Combust. Inst. **30**(2), 2929–2937 (2005)
Pappa, G.D., Perakis, C., Tsimpanogiannis, I.N., Voutsas, E.C.: Thermodynamic modeling of the vapor-liquid equilibrium of the CO_2/H_2O mixture. Fluid Phase Equilib. **284**(1), 56–63 (2009)
Patankar, S.V., Spalding, D.B.: Numerical Prediction of Flow, Heat Transfer, Turbulence and Combustion, pp. 54–73. Elsevier, Amsterdam (1983)
Peng, D.Y., Robinson, D.B.: A new two-constant equation of state. Ind. Eng. Chem. Fundam. **15**(1), 59–64 (1976)
Perakis, C., Voutsas, E., Magoulas, K., Tassios, D.: Thermodynamic modeling of the vapor-liquid equilibrium of the water/ethanol/CO_2 system. Fluid Phase Equilib. **243**(1–2), 142–150 (2006)
Pint, B.A., Keiser, J.R.: The effect of impurities on oxidation in supercritical CO2 at 750 C. Tech. rep., Oak Ridge National Lab. (ORNL), Oak Ridge, TN (United States) (2018)
Pohl, S., Jarczyk, M., Pfitzner, M., Rogg, B.: Real gas CFD simulations of hydrogen/oxygen supercritical combustion. Progr. Propul. Phys. **4**, 583–614 (2013)
Pope, S.B.: Ten questions concerning the large-eddy simulation of turbulent flows. New J. Phys. **6**(1), 35 (2004)
Ray, S., Raghavan, V., Gogos, G.: Two-phase transient simulations of evaporation characteristics of two-component liquid fuel droplets at high pressures. Int. J. Multiph. Flow **111**, 294–309 (2019)
Ribert, G., Petit, X., Domingo, P.: High-pressure methane-oxygen flames. analysis of sub-grid scale contributions in filtered equations of state. J. Supercrit. Fluids **121**, 78–88 (2017)
Robertson, E., Choudhury, V., Bhushan, S., Walters, D.K.: Validation of openfoam numerical methods and turbulence models for incompressible bluff body flows. Comput. Fluids **123**, 122–145 (2015)
Roy, A., Segal, C.: Experimental study of fluid jet mixing at supercritical conditions. J. Propul. Power **26**(6), 1205–1211 (2010)
Serrano, J., Piqueras, P., Navarro, R., Tarí, D., Meano, C.M.: Development and verification of an in-flow water condensation model for 3D-CFD simulations of humid air streams mixing. Comput. Fluids **167**, 158–165 (2018)
Smagorinsky, J.: General circulation experiments with the primitive equations: I. the basic experiment. Mon. Weather Rev. **91**(3), 99–164 (1963)
Smith, G.P.: Gri-mech 3.0. http://www.me.berkley.edu/gri_mech/ (1999)
Sod, G.A.: A survey of several finite difference methods for systems of nonlinear hyperbolic conservation laws. J. Comput. Phys. **27**(1), 1–31 (1978)
Somait, F.A., Kidnay, A.J.: Liquid–vapor equilibriums at 270.00 K for systems containing nitrogen, methane, and carbon dioxide. J. Chem. Eng. Data **23**(4), 301–305 (1978)
Star, A.M., Edwards, J.R., Lin, K.C., Cox-Stouffer, S., Jackson, T.A.: Numerical simulation of injection of supercritical ethylene into nitrogen. J. Propul. Power **22**(4), 809–819 (2006)
Stradi, B.A., Brennecke, J.F., Kohn, P., Stadtherr, M.A.: Reliable computation of mixture critical points. AIChE J. **47**(1), 212–221 (2001)
Su, L., Mungal, M.: Simultaneous measurements of scalar and velocity field evolution in turbulent cross-flowing jets. J. Fluid Mech. **513**, 1 (2004)
Takahashi, S.: Preparation of a generalized chart for the diffusion coefficients of gases at high pressures. J. Chem. Eng. Jpn. **7**(6), 417–420 (1975)
Tretola, G., Vogiatzaki, K., Navarro-Martinez, S.: Effect of the density ratio variation on the dynamics of a liquid jet injected into a gaseous cross-flow. Phys. Fluids **33**(9), 092,120 (2021)
Trujillo, M., Torres, D., O'Rourke, P.: High-pressure multicomponent liquid sprays: departure from ideal behaviour. Int. J. Eng. Res. **5**(3), 229–246 (2004)
Tudisco, P., Menon, S.: Numerical investigations of phase-separation during multi-component mixing at super-critical conditions. Flow Turbul. Combust. **104**(2), 693–724 (2020)
Tudisco, P., Menon, S.: A vapor–liquid equilibrium induced Lewis number effect in real-gas shear layers: a theoretical study. Phys. Fluids **32**(11), 112,111 (2020)

Tudisco, P., Menon, S.: Analytical framework for real-gas mixtures with phase-equilibrium thermodynamics. J. Supercrit. Fluids **164**, 104929 (2020)
Unnikrishnan, U., Wang, X., Yang, S., Yang, V.: in 53rd AIAA/SAE/ASEE Joint Propulsion Conference, p. 4855 (2017)
Unnikrishnan, U., Huo, H., Wang, X., Yang, V.: Subgrid scale modeling considerations for large eddy simulation of supercritical turbulent mixing and combustion. Phys. Fluids **33**(7), 075,112 (2021)
Vesely, L., Manikantachari, K., Vasu, S., Kapat, J., Dostal, V., Martin, S.: Effect of impurities on compressor and cooler in supercritical CO_2 cycles. J. Energy Resour. Technol. **141**(1), 012003 (2019)
Xu, N., Dong, J., Wang, Y., Shi, J.: High pressure vapor liquid equilibria at 293 K for systems containing nitrogen, methane and carbon dioxide. Fluid Phase Equilib. **81**, 175–186 (1992)
Xu, K., Ruan, B., Meng, H.: Validation and analyses of rans CFD models for turbulent heat transfer of hydrocarbon fuels at supercritical pressures. Int. J. Therm. Sci. **124**, 212–226 (2018)
Yan, C., Aggarwal, S.K.: A high-pressure droplet model for spray simulations (2006)
Yang, S., Li, Y., Wang, X., Unnikrishnan, U., Yang, V., Sun, W.: In 53rd AIAA/SAE/ASEE joint propulsion conference (2017), p. 4858
Yang, V.: Modeling of supercritical vaporization, mixing, and combustion processes in liquid-fueled propulsion systems. Proc. Combust. Inst. **28**(1), 925–942 (2000)
Yao, M.X., Hickey, J.P., Ma, P.C., Ihme, M.: Molecular diffusion and phase stability in high-pressure combustion. Combust. Flame **210**, 302–314 (2019)
Zhang, H., Yang, S.: in AIAA Scitech 2021 Forum (2021), p. 0549
Zhu, G.S., Reitz, R.D.: A model for high-pressure vaporization of droplets of complex liquid mixtures using continuous thermodynamics. Int. J. Heat Mass Transf. **45**(3), 495–507 (2002)